Dynamic healing-assembly for biocompatible, biodegradable, stretchable and self-healing triboelectric nanogenerators

Ao Shen[1], Huixia Xuan, Shijia Gu[1], Rasoul Esmaeely Neisiany[2,3], Wenmiao Shu[4], Wei Sun[1], Zhengwei You[1]**

[1]State Key Laboratory for Modification of Chemical Fibers and Polymer Materials, Institute of Functional Materials, College of Materials Science and Engineering, Donghua University, Shanghai 201620, China.

[2]Biotechnology Centre, Silesian University of Technology, Krzywoustego 8, 44-100 Gliwice, Poland

[3]Department of Polymer Engineering, Hakim Sabzevari University, Sabzevar 9617976487, Iran.

[4]Department of Biomedical Engineering, Wolfson Building, University of Strathclyde, 106 Rottenrow, Glasgow, G4 0NW, United Kingdom.

*Corresponding Author. E-mail: weisun@dhu.edu.cn (W. Sun); zyou@dhu.edu.cn (Z. You)

Abstract

Triboelectric nanogenerators (TENGs) have great potential as power sources for on-skin and implantable electronics. However, most existing TENGs are not suitable for the above applications due to limited material choices, often characterized by rigidity, susceptibility to damage, biological incompatibility, and non-biodegradability. Herein, we developed a simple self-healing assembly strategy based on introducing dynamic, supermolecular Cu(II)-dimethylglyoxime-urethane groups into a biocompatible and biodegradable polyurethane elastomer, to simultaneously address the above obstacles. The coordination of Cu^{2+} dynamic bonds significantly enhanced the mechanical properties of elastomer, resulting in a modulus of 9.4 MPa and toughness of 40.2 MJ/m^3. These bonds also gave the elastomer skin-like self-healing capabilities, achieving a healing efficiency of 77.5% at 80 ºC. Subsequently, a highly stretchable and integrated triboelectric nanogenerator (Cu-POU TENG) with self-healing capabilities was developed, based on Cu-POU technology. The Cu-POU TENG with an effective area of 1.5 × 1.5 cm^2 produced an open-circuit voltage of 38 V in single-electrode mode. The Cu-POU TENG could restore its original electrical properties through self-healing after mechanical damage. Furthermore, the Cu-POU TENG exhibited biocompatibility and biodegradability, making it suitable for on-skin and implantable electronics. Notably, the Cu-POU TENG maintained a stable voltage output throughout the degradation process. The integration

of self-healing features enabled a sophisticated structure, allowing the Cu-POU TENG to function effectively as a motion sensor for tracking body movement. This Cu-POU TENG holds great potential for applications in on-skin and implantable electronics.

Keywords: Triboelectric nanogenerators; biocompatibility, biodegradability; self-healing

1 Introduction

On-skin and implantable electronics have been a research hotspot as they can improve the quality of human life through health monitoring, physical training, and entertainment[1-6]. Triboelectric nanogenerators (TENGs) are employed as power sources and self-powered sensors for implantable and wearable electronics as a consequence of their uncomplicated structure, facile production, reasonable cost, and excellent output[7-9]. To meet the requirements of on-skin and implantable electronics, skin-comfort TENGs need to possess elasticity, sustainability, biocompatibility, and biodegradability[10-14]. During continuous use procedure, TENGs often suffer from fatigue and wear, resulting in damage to the friction layer. Additionally, accidental cuts or scratches could cause mechanical damage. These injures contribute to the deterioration of TENGs. Therefore, self-healing is another important property for TENGs to recover the performance after damage. However, the selection of materials for on-skin and implantable TENGs is limited. Compared to traditional rigid inorganic electronic materials, soft organic materials, such as widely used polymers like polydimethylsiloxane and polyamide, are more suitable[15-17]. However, these materials are nondegradable, leading to electronic waste. Consequently, various linear synthetic or naturally occurring biocompatible and biodegradable materials, such as polycaprolactone, polylactic acid, and cellulose, are employed to fabricate on-skin and implantable electronics with biodegradability performance [16, 18-22]. However, their application is limited due to their high modulus, restricted elasticity, and absence of self-healing properties. Therefore, certain degradable thermosetting elastomers like poly(glycerol sebacate) (PGS) and epoxidized soybean oil thermosets have been applied in wearable electronics[23-25]. Nevertheless, their covalent cross-linking structure poses challenges in processing and constructing complex 3D structures. To enhance performance, gels that encapsulate water or ionic liquids within the networks of the cross-linked polymers are extensively employed in the fabrication of wearable electrics. Despite possessing good biocompatible and self-healing properties, the long-term stability of hydrogel-based wearable

electronics has been always a big concern, since they are dehydrated easily as a consequence of water evaporation[26-28]. Although ionic liquids have a non-volatile nature, the ionic liquid leakage from the ionogels under large deformation has to be considered, which can cause adverse effects on human health[29-33]. Polyurethane has been widely used in the biomedical field because of its excellent molecular designability and performance tunability[34-36]. However, most polyurethanes applied to TENGs are not degradable or self-healing[37-39]. Consequently, it is still extremely necessary to solid-state and biodegradable polyurethane elastomers with self-healing properties as the biocompatible alternatives for on-skin and implantable electronics.

Herein, to address the aforementioned challenges, we developed a biocompatible and biodegradable polyurethane elastomer based on Cu(II)-dimethylglyoxime-urethane (Cu-DOU) group having triple dynamic bonds. This material simultaneously balances biodegradability, elasticity, and endows self-healing properties. Biodegradable polycaprolactone-diol (PCL-diol) was employed as the soft segment, PDI was employed as the hard segment, and dimethylglyoxime (DMG) acted as the chain extender. Then Cu^{2+} was coordinated with dimethylglyoxime-urethane (DOU) covalent bonds, to obtain Cu^{2+} coordinated polyurethane (Cu-POU). The developed Cu-POU exhibited biocompatibility, biodegradability, self-healing ability, and stretchability. The reversible dissociation and association of the oxime-urethane unit endowed the Cu-POU with the self-healing ability. The coordination interaction of copper ions and DMG unit improved the mechanical toughness and self-healing efficiency. Subsequently, an integrated TENG (Cu-POU TENG) was prepared having self-healing ability. With the Cu-POU as triboelectrification layer, the poly(3,4-ethylenedioxythiophene):polystyrenesulfonate (PEDOT:PSS) as electrode, the Cu-POU TENG worked in single-electrode mode. Cu-POU TENG recovered the original electrical properties through self-healing after mechanical damage and could maintain the voltage output during the degradation process. Moreover, the Cu-POU TENG can be prepared into sophisticated structures by self-healing properties. This TENG prepared with biocompatible material showed high potential to monitor human movements.

2 Experimental and methods

2.1 Materials

Dimethylglyoxime (DMG), copper (II) chloride ($CuCl_2$), and anhydrous diethyl ether were provided by Sinopharm Chemical Reagent. Polycaprolactone diol (PCL diol, M_n=2000) was purchased from Sigma-Aldrich. Pentamethylene diisocyanate (PDI) was provided by Henan Bon Industrial. N, N-dimethylformamide (DMF, anhydrous) was provided by J&K Chemical. The aqueous PEDOT:PSS solution was provided by Clevios™ PH1000, Heraeus Electronic Materials.

2.2 Synthesis of POU

PCL diol (10 g, 5 mmol) was vacuumed in a round-bottomed flask at 110 ºC for 2 hours to remove water. After the mixture was cooled to 70 ºC, DMF (8 mL) and PDI (1.54 g, 10 mmol) were sequentially added to the mixture. The reaction proceeded for 4 hours at 70 ºC in a nitrogen atmosphere. Subsequently, DMG (0.58 g, 5 mmol) dissolved in 8 mL DMF was added to the mixture. The mixture reacted for another 15 h under the same conditions. The resulting product was precipitated in anhydrous diethyl ether and stirred to obtain a white precipitate. Lastly, the resulting precipitate was transferred to a vacuum oven at 50 ºC and kept for 24 hours to obtain POU.

2.3 Preparation of Cu-POUs

The Cu-POU was synthesized via DMG units in POU coordinating with Cu^{2+} (Fig. 1a) according to our previously reported work[40]. By mixing POU with different amounts of $CuCl_2$, Cu-POU 25%, 50%, and 75% were prepared. Taking the Cu-POU 25% as an example, POU (5 g, containing 2.063 mmol DMG), $CuCl_2$ (34.7 mg, 0.258 mmol), and DMF (8 mL) were stirred in a round-bottomed flask and then the mixture was cast in a Teflon dish. Subsequently, the dish was vacuum dried at 50 ºC for 48 h to get the Cu-POU 25% film. The Cu-POU 50% and Cu-POU 75% films were also prepared with a similar procedure and change in the feed mole number of $CuCl_2$. Cu-POU 50% has the same amount of POU (5 g, containing 2.063 mmol DMG), and twice the amount of $CuCl_2$ (69.4 mg, 0.516 mmol). While Cu-POU 75% consists of POU (5 g, containing 2.063 mmol DMG) and $CuCl_2$ (106.1mg, 0.774 mmol).

2.4 Chemical and Morphological Characterizations of POU and Cu-POUs

All tests were conducted at ambient conditions unless otherwise noted. ^{1}H-nuclear magnetic resonance (^{1}H-NMR) spectra were recorded by a Bruker Avance 600 NMR spectrometer (GmbH,

Germany). The molecular weight was characterized by a GPC-50, (Polymer Laborato, China). Hexafluoroisopropanol (HFIP) was utilized as the eluent, while its flow rate was set at 0.6 mL min^{-1}. Attenuated total reflectance Fourier transform infrared spectroscopy (ATR-FTIR) tests were performed by a Nicolet 8700 spectrometer (Thermo Electro Corporation, USA) in the wavelength ranging from 4000 cm^{-1} to 500 cm^{-1} with ATR accessory. Differential scanning calorimetry (DSC) characterizations were carried out by a DSC Q20 (TA, USA) under a nitrogen atmosphere, while the heating rate of the experiments was adjusted at 5 ºC min^{-1}. For the morphological characterizations, a scanning electron microscope (SEM) (SU8010, HITACHI, Japan) with 1 kV voltage and 10 μA current was employed. Before the observations, the samples firstly were mounted on aluminum stubs and gold-sputtered.

2.5 Mechanical properties of the synthesized POU and Cu-POUs

The mechanical properties of the synthesized POU and Cu-POU elastomers were measured by a universal testing machine MTS Echo (Exceed 40, USA) equipped with a 100 N load cell and TestSuite TW software[41]. The POU and Cu-POUs films were cut into strips with a width of 4 mm and a length of 20 mm. The thickness of the strips was measured by a micrometer. The uniaxial tensile test was tested at a tensile rate of 50 mm min^{-1}. The Young's modulus, ultimate tensile strength, and strain at failure were determined. At least three specimens were examined for each sample to calculate the averaged values. Cyclic tensile tests were also performed for 10 cycles at a crosshead speed of 50 mm min^{-1} and a recovery rate of 20 mm min^{-1}.

2.6 Self-healing property of POU and Cu-POU 25%

The self-healing property was evaluated by the scratch recovery and restoration of mechanical characteristics[42]. Scratch recovery tests were performed by scratching films with a blade and recovering the films at 80 ºC. An optical microscope (MDA2000, Future Optics) was used to observe the changes in the scratched films. The restoration of mechanical properties was determined by splicing the two individual cut specimens over a specified time at 80 ºC.

2.7 *In vitro* degradation of POU and Cu-POU 25%

In vitro degradation was tested by enzymatic degradation with thermomyces lanuginosus lipase

enzyme (20,000 U g^{-1}, Adamas life) in PBS solution[43]. The lipase enzyme solution was at an activity of 2000 U mL^{-1}. Samples (n=4) were weighed and immersed in 1 mL lipase solution, then incubated at 37 ºC. The samples were washed with deionized water and freeze-dried under a vacuum for a certain time. The degree of degradation was determined by the mass change.

2.8 Biocompatibility of POU and Cu-POUs

To measure the biocompatibility, the POU and Cu-POUs samples were immersed in Dulbecoo's modification Eagle's medium (DMEM) at 37 ºC and with 5% CO_2 in air for 48 h to obtain extracts. The extracts were then filtered and sterilized. Cell viability was tested by fibroblast through the CCK-8 cell viability assay (Dojindo Lab, Japan)[44]. DMEM medium was used as a control sample. Fibroblasts were seeded on 96-well plates and cultivated with extracts and DMEM medium for 24 hours. Afterward, CCK-8 assay was performed according to the manufacturer's instructions to assess cell viability. The optical density (OD) value was determined spectrophotometrically at 450 nm by a microplate reader (Thermo Fisher Scientific, USA). Four replicates were used for each sample. The OD ratio was calculated by the following formula:

$$\text{OD ratio} = (OD_{sample} - OD_{blank}) / (OD_{control} - OD_{blank}) \times 100\%$$

OD_{sample} was the OD value of fibroblasts cultivated with extracts. $OD_{control}$ was the OD value of fibroblasts cultivated with medium, and OD_{blank} was the OD value of the blank medium.

To further measure the biocompatibility, the fibroblast cell Live/Dead staining was carried out. Fibroblasts were seeded on sterilized POU and Cu-POU films at a density of 1.0×10^6 cells and incubated with Dulbecco's modified eagle medium (DMEM) for 24 h. Then images of dead cells (red fluorescence) and living cells (green fluorescence) were recorded using a confocal laser scanning microscopy (CLSM) (LSM 800, Zeiss, German).

2.9 Fabrication of the Cu-POU TENG

The Cu-POU 25% film was fixed on a polytetrafluoroethylene (PTFE) plate by two clips under a 50% pre-stretched state. The aqueous PEDOT:PSS solution was coated onto the pre-stretched film and then dried at room temperature overnight. After release, the wrinkled PEDOT:PSS electrode on the Cu-POU membrane was acquired. As an electrical connection, a copper line was then installed

onto the electrode for the electrical measurements. The electrode was encapsulated by another Cu-POU 25% film via self-healing to obtain the Cu-POU TENG.

2.10 Electrical performance evaluation of Cu-POU TENG

The resistance of the PEDOT:PSS electrode was measured by a Keithley DMM7510 multimeter (Keithley, USA). The Cu-POU TENG was fabricated with the size of 15×15×0.5 mm×mm×mm. To simulate the skin touching, the typical electrical output performance of the Cu-POU TENG was evaluated by an electrometer 6514 instrument (Keithley, USA) with hogskin. A durability test of the Cu-POU TENG was performed as the time was set to 800 s.

3 Results and discussion

3.1 Synthesis and characterization of POU and Cu-POU

Fig. 1a presents the synthesis procedure of the POU from PCL-diol, DMG, and PDI. PCL-diol was employed as the soft segment due to its biodegradability. PDI was utilized as the hard segment because of biological derivation. DMG acting as the chain extender was the key in the design of POU and Cu-POU. It introduced reversible DOU groups and formed the basis of dynamic covalent networks. The hard segment crystallization was inhibited by the methyl groups in DMG to facilitate the chain motions[45, 46]. Furthermore, the nitrogen atoms in adjacent oxime groups of DMG can readily chelate metal ions such as Cu^{2+} to form a complex[41]. Accordingly, the reversible DOU covalent bonds, hydrogen bonds, and Cu-DOU coordination bonds constitute triple dynamic bonds. The dissociation of Cu-DOU coordination bonds and hydrogen bonds, weaker bonds, leads to a significant dissipation of energy during mechanical deformation and results in high toughness[47]. Simultaneously, the strong covalent bonds contribute to the structural integration to ensure mechanical stability. The reassociation of weaker bonds results in rapid self-healing. Simultaneously, coordination of Cu^{2+} improves the DOU group exchange reaction to facilitate self-healing once it is damaged[40, 42]. In a word, as shown in Fig. 1d the synergetic effect of hybrid triple networks contributes to the simultaneous outstanding mechanical properties and self-healing.

The successful synthesis of POU was confirmed by ^{1}H-NMR analysis (Fig. 1b). The observed

chemical shifts at 7.56-7.63 ppm (a) and 6.98-7.05 ppm (b) were ascribed to the imine linkage protons. The proton peak at 2.18 ppm (c) was associated with the protons of the DMG segment[40, 48]. The additional peaks detected at 4.21, 4.05-3.97, 2.33-2.25, 1.59-1.48, 1.33-1.23 ppm corresponded to PCL. Subsequently, the molecular weight of the synthesized Cu-DOU was assessed using GPC. The number-average molecular weight (M_n) was acquired to be 14.9 k, with a polydispersity index (PDI) of 2.27.

Abundant DMG units in POU can coordinate with Cu^{2+} to form Cu-POU complexes. By mixing POU with several amounts of Cu^{2+}, Cu-POU 25%, 50%, and 75% were prepared. The chemical structure of POU and Cu-POU was characterized by ATR-FTIR, and the results are shown in Fig. 1d and e. The peaks centered at 1723 cm^{-1} and 3378 cm^{-1} were associated with C=O and N-H stretching vibrations of urethane groups respectively, confirming the successful synthesis of urethane groups. Notably, no peaks corresponding to –N=C=O, attributed to PDI, were observed within the range of 2240-2280 cm^{-1}. Additionally, the peaks of the N-O bond displayed a reduced intensity and a slight shift from 973.4 cm^{-1} to 975.3 cm^{-1} after coordination, affirming the Cu^{2+} and "N" atom coordination interaction(Fig. 1e) [40].

The glass transition temperature (T_g) of the four elastomers (POU, Cu-POU 25%, Cu-POU 50%, and Cu-POU 75%) was assessed by the DSC evaluations. As presented in Fig. 1f and g, T_g of the Cu-POU elastomers after coordination of Cu^{2+} were all decreased compared to the pure POU, which could be attributed to the increase in microphase separation. Cu^{2+} coordinated oximido deriving from different molecules, thus affected the arrangement of polymer molecules, enhanced the degree of aggregation of the hard segment, and consequently reduced the dispersion between the hard and soft segments [48, 49].

The hydrophilicity of the material is advantageous for its application in the on-skin and implantable electronics. As depicted in Fig. 1h-l, the addition of Cu^{2+} enhanced surface hydrophilicity, reducing the water contact angle from 85.0±2.3 º to 63.4±0.2 º.

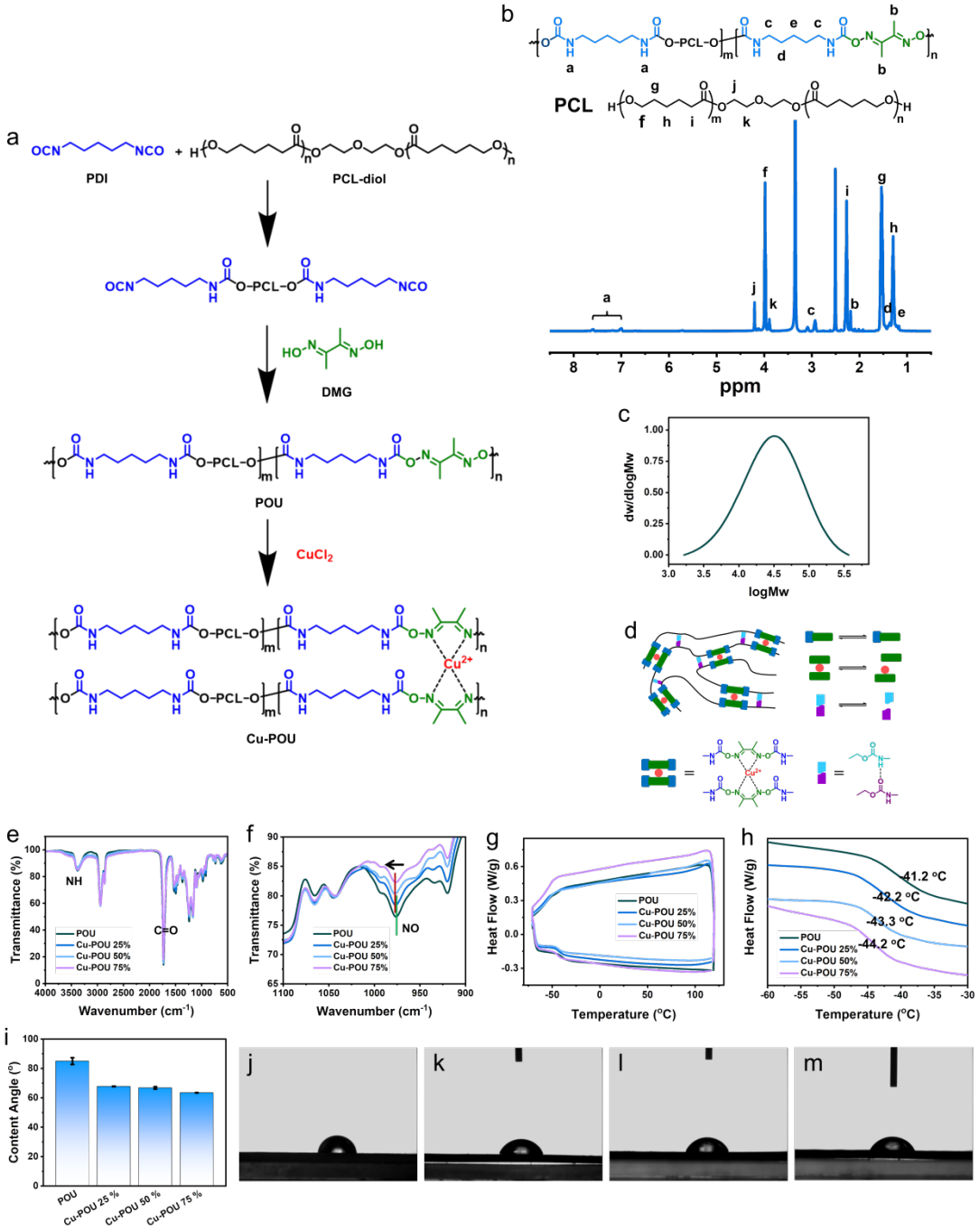

Fig.1 (a) The chemical route for the design and preparation of POU and Cu-POU. (b) The structure and ^{1}H NMR spectrum of POU. (c) Schematic representation of Cu-POU chemical structure. Triple dynamic bonds including reversible covalent (deep blue and green rectangles), Cu^{2+}-ligand (red circle), and hydrogen bonds (light blue and purple polygons) provided hybrid dynamic networks. (d, e) The FT-IR spectra of POU and Cu-POU. (f, g) DSC curves of POU and Cu-POU at the temperature range from −70 to 120 °C. (h) Water content angle of POU and Cu-POU films. (j-m) Digital images of water contact angles of (i) POU, and Cu-POU (j) 25%, (k) 50% and (l) 75% films.

3.2 Mechanical and self-healing performance of POU and Cu-POU

The mechanical characteristics of the synthesized elastomers were evaluated through uniaxial tensile tests (Fig. 2). Fig. 2a presents the typical stress-strain diagrams of the synthesized elastomers. With the introduction of Cu^{2+} in the POU, both tensile strength and toughness of the Cu-POU 25% significantly increased, reaching values 1.13 and 1.82 times those obtained for POU, respectively. However, with Cu^{2+} content increased to 50%, the tensile strength and toughness decreased to 0.49 and 0.37 times of POU. When the content of Cu^{2+} increased to 75%, tensile strength and toughness were 0.58 and 0.36 times of POU (Fig. 2b). The coordination of Cu^{2+} at a small amount was expected to enhance the strength and toughness by increasing the intermolecular coordination crosslinking. Moreover, the energy dissipation of dynamic cross-link points upon loading increased. This enhancement might stem from the increase in hidden length resulting from the folding of further polymeric chains triggered by Cu-DOU coordination bonds[42, 50]. The covalent networks and dual sacrificial links were expected to provide Cu-POU having great toughness as well as good elasticity. While, with more increase in Cu^{2+} content, the mechanical properties of Cu-POU 50% and 75% diminished. This decline might be attributed to the larger amount of incompletely cross-linked metal salts, leading to a reduction in mechanical properties as the Cu^{2+} concentration increased[51]. Above all, the Cu-POU 25% was identified as the optimal composition. Cu-POU 25% displayed remarkable resilience. As shown in Fig. 2c, cyclic tensile tests with gradually larger strains were carried out without waiting intervals between two loadings. Initially, with a small strain (100%) in the first tensile cycle, the covalent networks and the unbroken dynamic bonds, including Cu-DOU coordination bonds and hydrogen bonds, entropically pushed the networks to return almost entirely to their initial stage. This demonstrated Cu-POU 25% as a robust elastomer within the 100% strain, suitable for numerous practical applications. Subsequent cycles with larger strains exhibited more noticeable residual strain in Cu-POU 25%, attributable to the reformation of ruptured dynamic bonds throughout stretching. The successful energy dissipation can be recognized from the hysteresis loops[42]. Furthermore, repeated cyclic tensile tests (Fig. 2d) showcased a significant hysteresis loop in the first cycle, signifying substantial dissipation of energy. Whereas, in the second cycle, the energy dissipation notably decreased due to insufficient time for the broken sacrificial bonds to fully restore to their original state. Throughout the sequential tests, the hysteresis loop

exhibited a slight reduction, indicating an ongoing reorganization of sacrificial bonds[41].

The self-healing capability of the Cu-POU is crucial for recovering the sensing and energy output performance of the resultant TENG after damage[52, 53]. The films were scratched with a utility knife. After a 4-hour healing process at 80 ºC, the scratch on the surface of Cu-POU 25% film almost disappeared (Fig. 2f), while that on POU was still obvious (Fig. 2e). The self-healing ability of Cu-POU 25% at 80 ºC was also evaluated by tensile test (Fig. 2g-i). After being cut and healing, Cu-POU 25% showed a higher recovery stage in fracture strain and tensile strength in comparison with pure POU. After being cut and healing, the fracture strain and tensile strength of Cu-POU 25% recovered to 52.0% for 6 hours and 77.5% for 12 hours, respectively (Fig. 2g). While those acquired for POU only recovered to 22.5% for 6 hours and 50.9% for 12 hours (Fig. 3h). For demonstration, two pieces of Cu-POU 25% film can be integrated and resist bending, twisting, and stretching (Fig. 2k) after self-healing for 12 h at 80 ºC. These results highlighted the significant role of Cu-DOU coordination interaction in the self-healing process (Fig. 2j). The presence of triple dynamic bonds in Cu-POU 25%, including hydrogen bonds, Cu-DOU coordination bonds, and reversible DOU covalent bonds facilitated efficient self-healing following damage by promoting reassociation.

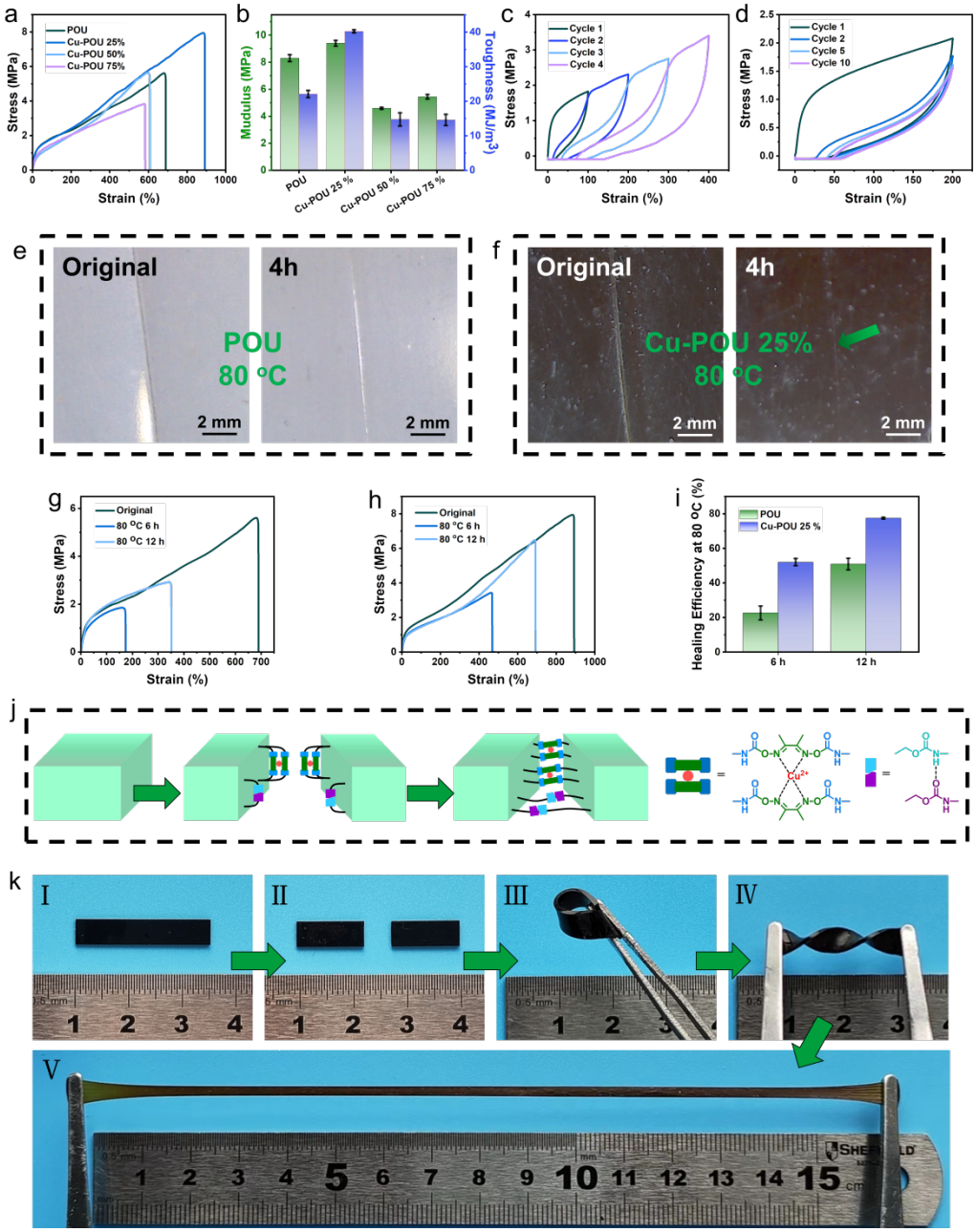

Fig. 2 (a) Tensile stress–strain curves of POU and Cu-POUs films. (b) The tensile Young's modulus and toughness of synthesized elastomers (n=3). (c) Sequential cyclic tensile curves of Cu-POU 25% film with different strains without waiting time. (d) Repeated cyclic tensile curves of Cu-POU 25% at 200% strain for 10 cycles. (e) Optical microscopy images of scratched and healed (e) POU and (f) Cu-POU 25% films after 4 h healing at 80 ℃. (g) Tensile stress-strain diagrams of original and healed (g) POU and (h) Cu-POU 25% films after 6 and 12 h healing at 80 ℃. (i) The healing efficiency of the POU and Cu-POU 25% films determined from fracture strain for the samples healed at 80 ℃. (j) The schematic representation of the self-healing process of Cu-POU. (k)

Photographs of the self-healing procedure of Cu-POU 25%. The healed film could be bent, twisted, and stretched.

3.3 *In vitro* degradation and biocompatibility of POU and Cu-POUs

Biodegradability is one of the key points of the materials for on-skin and implantable wearable electronics. To assess the biodegradability of the synthesized elastomers, the *in vitro* degradation experiments were carried out by immersing the samples in a PBS solution with 2000 U mL^{-1} lipase enzyme. The POU and Cu-POU 25% films showed moderate degradation of 52.9 ± 1.6% and 54.6 ± 1.8% total mass loss within 13 days, respectively (Fig. 3a). By the 14^{th} day, the films had disintegrated, making collection challenging. Notably, during degradation, micropores appeared on the material surfaces (Fig. 3i-l). Simultaneously, there was a decline in mechanical strength and self-healing ability (Fig. 3b-d). After 3 and 5 days of immersion, the fracture strain of Cu-POU 25% films decreased from 888.0 ± 15.5% to 734.3 ± 78 and 341.3 ± 15.9% respectively. Additionally, the self-healing efficiency based on fracture strain was measured to be 74.5 and 49.3%, respectively. This decrease was associated with the reduction of the DMG unit, evident in the decline of the -N-O peak at 975.3 cm^{-1} in FT-IR (Fig. 3m, n). During the degradation process, the material underwent a change in quality, while effectively retaining a certain mechanical strength and self-healing ability. This characteristic was advantageous for ensuring long-term reliability throughout the application process.

The safety of the POU and Cu-POU was also determined prior to on-skin and implantable applications by CCK-8 analysis using fibroblasts in the extracts (Fig. 3o). No difference in optical density (OD) values between POU, Cu-POU 25%, Cu-POU 50%, and the control group was observed, indicating no significant difference in cell viability[54, 55]. The OD value of Cu-POU 75% was lower than other samples, which can be ascribed to the excessive Cu^{2+} toxic to cells. The POU and Cu-POU were added to the fibroblasts medium and cultivated for 24 h， the green fluorescence was strong, indicating high cell viability (Fig. 3p). These results indicated that PU, Cu-POU 25% and Cu-POU 50% had no evident direct cytotoxicity for fibroblasts[12, 56]. The excellent biocompatibility makes them suitable for on-skin and implantable electronics.

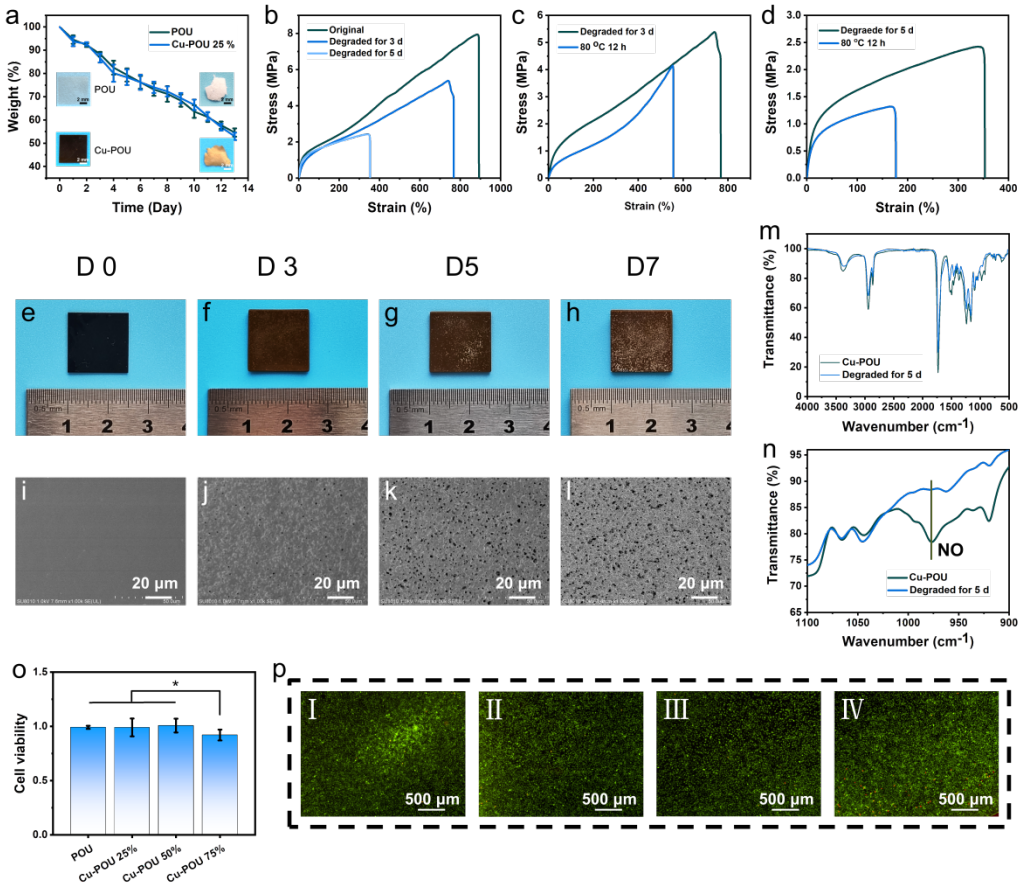

Fig. 3 (a) *In vitro* enzymatic degradation of POU and Cu-POU 25% samples at 37 ºC (n=4). (b) The tensile stress–strain curves of Cu-POU 25% after 3 and 5 days of immersion. (c) The typical tensile stress-strain curves of original and healed of (c) 3 days and (d) 5 days immersed Cu-POU 25%, healed for 12 h at 80 ºC. (e-l) Optical microscopy images of the Cu-POU 25% film during degradation programs. (i-l) Surface morphology of the Cu-POU 25% film recorded by SEM during degradation programs. (m, n) The FT-IR spectra of Cu-POU 25% before and after 5 days of degradation. (o) Cell viability of POU and Cu-POU. The data were expressed as mean ± standard deviation. Statistical significance compared with the control group was marked as * $p < 0.05$. (p) LIVE/DEAD cell images of PU and Cu-POU, recorded by CLSM (I - POU, II - Cu-POU 25 %, III - Cu-POU 50 %, IV - Cu-POU 75 %).

3.4 Triboelectric Performance of Cu-POU 25% Based TENGs

Cu-POU TENG comprised Cu-POU 25% and PEDOT:PSS. The process involved coating the PEDOT:PSS solution onto a pre-stretched Cu-POU 25% film, which was subsequently dried.

Following the release, the PEDOT:PSS electrode was installed with a copper line and encapsulated by another Cu-POU 25% film through self-healing to create the integrated Cu-POU TENG (Fig. 4a). To assess the output performance of the TENG, a hogskin was used to simulate human skin with an area of 1.5×1.5 cm^2. The electrical output of the Cu-POU TENG was measured for several frequencies and shown in Fig. 4d-f. With the motion frequency varying from 1-4 Hz, no obvious output changes in V_{OC} (open-circuit voltage) and Q_{SC} (short circuit transfer charge) were observed, showing peak values at about 40 V and 13 nC (Fig. 4e, g). A significant increase in I_{SC} (short-circuit current) was detected from 0.53 μA to 0.95 μA (Fig. 4f). It could be ascribed to the increase of friction layer movement rate with the rise of work frequency. As a result, the electron transfer rate became faster, then a higher current output was obviouse[57]. The Cu-POU TENG operated in a single-electrode mode (Fig. 4h) [12, 57, 58]. At first, the two friction layers (the TENG and skin) were separated, with no electrical output. When applied vertical pressure, the TENG contacted the skin, the contact electrification effect led to the transfer of electrostatic charges from the skin to the surface of Cu-POU TENG till saturation (I). As the pressure released, the TENG moved away from the skin, the triboelectric charges built an electrostatic field. Then the electrostatic field drove the electrons to flow from the electrode to the reference electrode (ground), through the external load during the process. This led to the free electron accumulation in the electrode. It kept going until it was balanced (II, III). Once the TENG approached the skin once more, electrons flowed from the ground toward the electrode, resulting in a reversed electric output signal (IV).

In practical applications, stability and durability are important for TENGs. To assess durability and stability, the electrical output voltage was examined for 1500 seconds (equivalent to 4500 cycles) (Fig. 4i). The voltage remained sustained with no significant attenuation, indicating durability and reliability during application. The self-healing performance of Cu-POU also improved the durability of the Cu-POU TENG. After scratching the surface of the TENG, the V_{OC} output decreased to 76.3% (29 V) of its original value (38 V) at 3 Hz, while, after the self-healing process, the V_{OC} recovered to 36 V (Fig. 4k). The Cu-POU TENG could recover the original electrical properties through self-healing after mechanical damage and the Cu-POU TENG maintained the voltage output during the degradation process. The self-healing property of Cu-POU TENG contributed to its ability to recover the original electrical properties after mechanical damage, thereby extending the service life of the TENG. Moreover, by utilizing self-healing, Cu-POU TENG can be configured into

sophisticated structures to enhance signal strength. In the future, Cu-POU TENG can be assembled to more complex structure by combining with 3D printing to further improve the performance. The roughness of friction layer can significantly affect the performance of TENG. The rougher the surface of friction layer, the stronger the electrical signal[59]. After degradation in a PBS solution with 2000 U mL^{-1} lipase enzyme, the V_{OC} of the Cu-POU TENG slightly increased at the frequency of 3 Hz due to the increased roughness of the surface (Fig. 4j), indicating the stability of signal output during degradation[60].

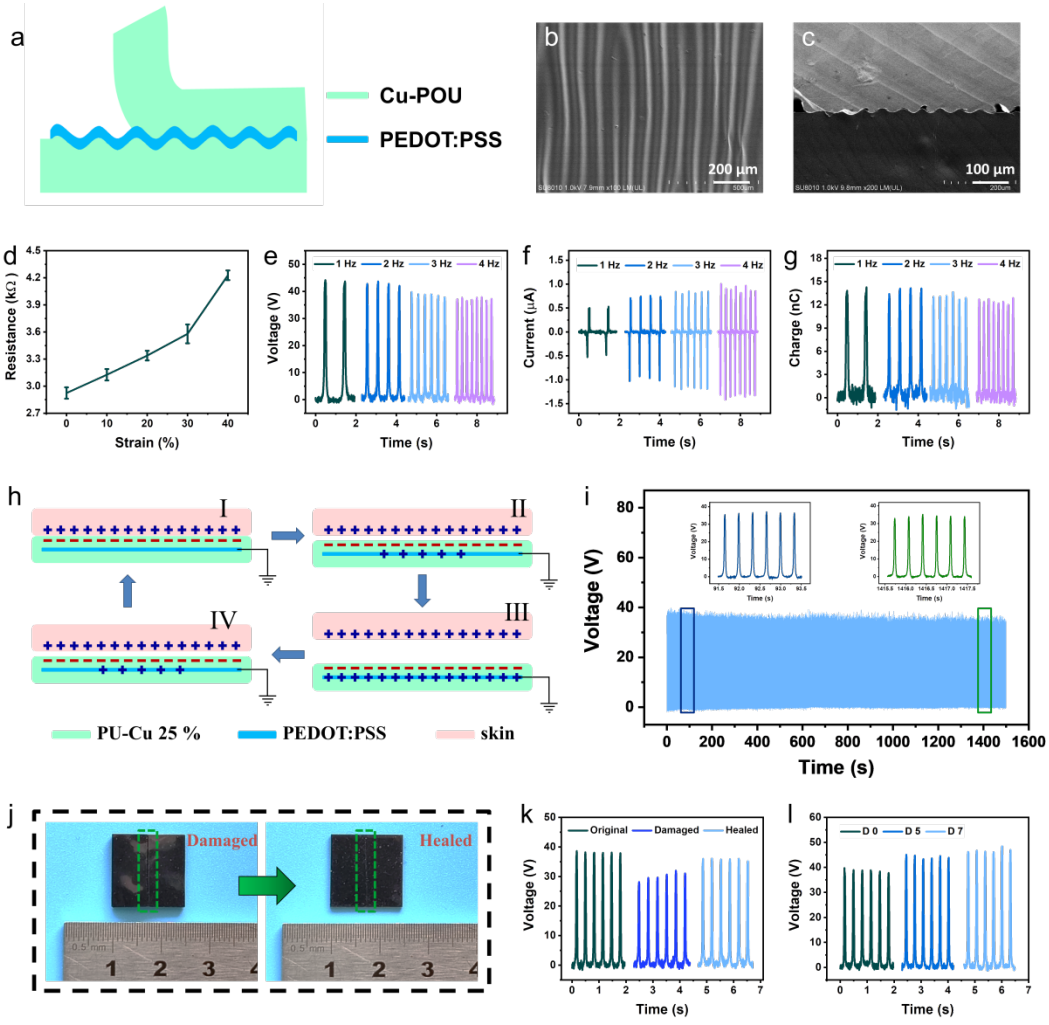

Fig. 4 (a) Schematic diagram of the Cu-POU TENG. (b, c) SEM images of a wrinkled PEDOT:PSS film on Cu-POU 25% film. (d) Resistance of the PEDOT:PSS electrode under different tensile strains. (e-g) Electrical outputs of the (e) V_{OC}. (f) I_{SC}. (g) Q_{SC}. (h) Schematic illustration of the working mechanism of the prepared TENG. (i) Long-term stability and durability test results of the Cu-POU TENG. (j) Photographs of the scratched and healed Cu-POU TENG. (k) The V_{OC} of the

original, scratched and healed Cu-POU TENG. (l) The V_{OC} of the Cu-POU TENG before and after 5, 7 days of degradation in lipase enzyme with a frequency of 3 Hz.

3.5 Application of Cu-POU TENG as Self-Powered Sensors

In the application, self-powered sensors not only requires that the material has excellent mechanical properties, but also needs high sensitivity to improve the application value [61, 62]. The Cu-POU TENG demonstrated remarkable characteristics, encompassing stretchability, self-healing ability, biocompatibility, biodegradation, and the capacity to exhibit distinct electrical signals under varied mechanical impact and deformation. However, its initial attachment to the skin resulted in weak signal recognition, for instance when the wrist was bent at a 90-degree angle (Fig. 5e-f). To fortify the interaction between the Cu-POU TENG and the skin, small pieces were strategically assembled at four corners by integrating self-healing capabilities. Consequently, the Cu-POU TENG effectively operated as a motion sensor for monitoring human movement (Fig. 5a-b). Real-time signals of body movements were recorded by the Cu-POU TENG, underscoring its potential as a motion sensor. Specifically focused on monitoring wrist motion, the Cu-POU TENG displayed a triboelectric voltage during wrist movements up and down. Notably, as the wrist bent, increasing from 45 degrees to 90 degrees, the V_{OC} increased from 0.05 V to 0.09 V (Fig. 5g, h). The schematic diagram of how the Cu-POU TENG transmits signals was depicted in Fig. 5d. Initially, when TENG and skin were separated, there was no electrical output. When the joint bended, the TENG contacted the skin, the contact electrification effect caused the transfer of electrostatic charges from the skin to the surface of Cu-POU TENG until saturation (I). As the joint relaxed and the TENG moved away from the skin, the triboelectric charges generated an electrostatic field, driving electrons to flow from the electrode to the reference electrode (ground), through the external load. This process leads to the accumulation of free electrons in the electrode until equilibrium is reached (Ⅱ, Ⅲ). Subsequently, as the TENG approaches the skin again, electrons flow from the ground toward the electrode, resulting in a reversed electric output signal (Ⅳ).

Take wrist signal output as an example, when the wrist was not bended, there was no electrical output. As the wrist bended, the skin impacted with Cu-POU TENG, thus electrical output. As the degree of wrist bending increased, the contact area between skin and Cu-POU TENG increased, the

electrical output increased (Fig 5g, h). Similarly, observations when attached to the elbow and finger exhibited analogous trends. Where it was affixed to the elbow, the V_{OC} increased from 0.1 V to 0.15 V, and further to 0.6 V as the elbow bent from 45 degrees to 90 degrees, and eventually to 180 degrees (Fig. 5i, j). Additionally, the V_{OC} increased from 0.06 V to 0.16 V as the elbow and finger were bent from 90 degrees to 145 degrees (Fig. 5l, m). Analysis of the voltage output enabled the recognition of human joint motion and extraction of the precise motion frequency. Notably, the output frequency escalated in correlation with the bending frequency, irrespective of attachment to the elbow or finger (Fig. 5k, n). In summary, the versatile sensing capabilities of Cu-POU TENG present numerous practical applications across domains such as sports, entertainment, and beyond.

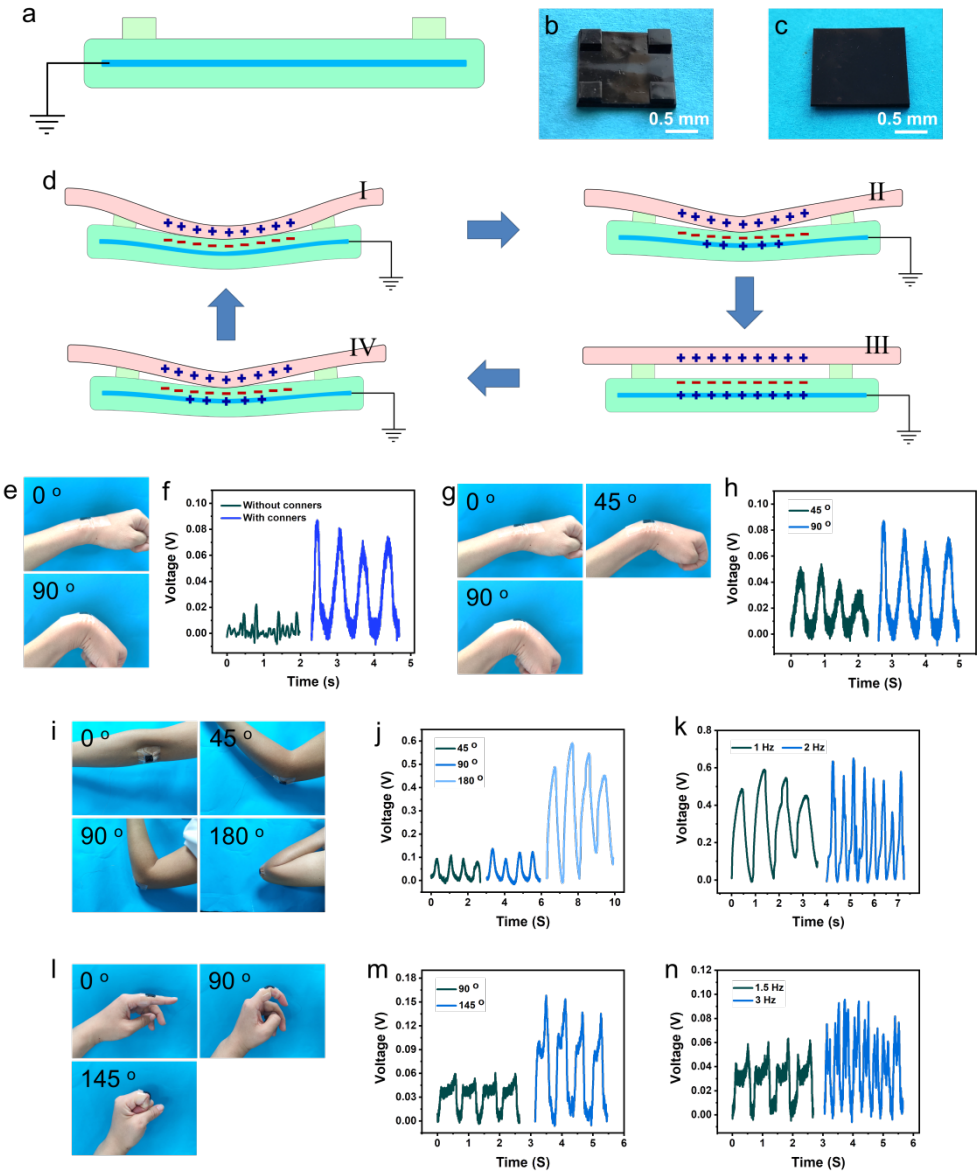

Fig. 5 (a) Schematic diagram of the active motion sensor to monitor human body movement. (b) Photograph of the Cu-POU TENG based active motion sensor with small pieces adhered at four corners. (c) Photograph of the Cu-POU TENG without small pieces. (d) Schematic illustration of the signals transmitting mechanism when Cu-POU TENG applied on skin. (e) The digital photo of the wrist with 90 º bending. (f) V_{OC} of the Cu-POU TENG with and without small pieces adhered at four corners on the wrist with 90 º bending. (g) The digital photo of the wrist with 45 º and 90 º bending. (h) V_{OC} of the Cu-POU TENG caused by bending the wrist at different angles. (i) The digital photo of the elbow with 45 º, 90 º, and 180 º bending. (j) V_{OC} caused by bending the elbow at different angles. (k) V_{OC} caused by bending the elbow at different frequencies with 180 º bending. (l) The digital photo of the finger with 90 º and 180 º bending. (m) V_{OC} caused by bending the finger at different angles. (n) V_{OC} caused by bending finger at different frequencies with 90 º bending.

4 Conclusion

In summary, to meet the requirements of on-skin and implantable electronics, we developed a biocompatible and biodegradable polyurethane elastomer based on Cu(II)-dimethylglyoxime-urethane (Cu-DOU) groups with triple dynamic bonds. This method simultaneously balanced biodegradability, elasticity, and induced self-healing ability. Subsequently, we fabricated a stretchable integrated Cu-POU TENG through self-healing performance. Cu-POU TENG recovered the original electrical properties through self-healing after mechanical damage, and maintained the stability of signal output during degradation, confirming the stability and durability of the developed TENG in practical biological applications. Moreover, the Cu-POU TENG was prepared into a sophisticated structure with self-healing properties, effectively functioning as a motion sensor to monitor human movement when attached to the skin. This Cu-POU TENG showed a promising potential for on-skin and implantable electronics.

Declaration of Interest Statement

The authors declare that they have no known competing financial interests or personal relationships that could have appeared to influence the work reported in this paper.

Acknowledgments

This study was financially supported by the National Key Research and Development Program of China (2021YFC2400802, 2021YFC2101800)，the National Natural Science Foundation of China (52173117, 52002059, 21991123), Ningbo 2025 Science and Technology Major Project (2019B10068), Science and Technology Commission of Shanghai Municipality (20DZ2254900 and 20DZ2270800).

References

[1] H. Ling, R.W. Chen, Q.B. Huang, F. Shen, Y.Y. Wang, X.H. Wang, Transparent, flexible and recyclable nanopaper-based touch sensors fabricated via inkjet-printing, Green Chemistry 22(10) (2020) 3208-3215. https://doi.org/10.1039/d0gc00658k.

[2] Z. Wang, S.C. Yao, S.B. Wang, Z.R. Liu, X.Y. Wan, Q.H. Hu, Y.C. Zhao, C. Xiong, L.L. Li, Self-powered energy harvesting and implantable storage system based on hydrogel-enabled all-solid-state supercapacitor and triboelectric nanogenerator, Chemical Engineering Journal 463 (2023) 142427. https://doi.org/10.1016/j.cej.2023.142427.

[3] Y.P. Shi, X.L. Wei, K.M. Wang, D.D. He, Z.H. Yuan, J.H. Xu, Z.Y. Wu, Z.L. Wang, Integrated All-Fiber Electronic Skin toward Self-Powered Sensing Sports Systems, ACS Applied Materials & Interfaces 13(42) (2021) 50329-50337. https://doi.org/10.1021/acsami.1c13420.

[4] J. Yan, M.D. Lv, Y.B. Qin, B.J. Wang, W.M. Kang, Y.F. Li, G. Yang, Triboelectric Nanogenerators Based on Membranes Comprised of Polyurethane Fibers Loaded with Ethyl Cellulose and Barium Titanate Nanoparticles, ACS Applied Nano Materials 6(7) (2023) 5675-5684. https://doi.org/10.1021/acsanm.3c00124.

[5] Q.F. Shi, Z.X. Zhang, T. Chen, C.K. Lee, Minimalist and multi-functional human machine interface (HMI) using a flexible wearable triboelectric patch, Nano Energy 62 (2019) 355-366. https://doi.org/10.1016/j.nanoen.2019.05.033.

[6] K.X. Hou, S.P. Zhao, D.P. Wang, P.C. Zhao, C.H. Li, J.L. Zuo, A Puncture-Resistant and Self-Healing Conductive Gel for Multifunctional Electronic Skin, Advanced Functional Materials 31(49) (2021) 202107006. https://doi.org/10.1002/adfm.202107006.

[7] D.L. Yan, J. Ye, Y.H. Zhou, X.X. Lei, B. Deng, W.L. Xu, Research Progress of Fabrics with Different Geometric Structures for Triboelectric Nanogenerators in Flexible and Wearable Electronics, Advanced Fiber Materials 5(6) (2023) 1852-1878. https://doi.org/10.1007/s42765-023-00334-z.

[8] X.H. Zhang, J.W. Xu, X.M. Zhang, G.J. Chao, Q.X. Cao, T.X. Liu, Y. Liu, Simultaneous Evaporation and Foaming for Batch Coaxial Extrusion of Liquid Metal/Polydimethylsiloxane Porous Fibrous TENG, Advanced Fiber Materials 5(6) (2023) 1949-1962. https://doi.org/10.1007/s42765-023-00314-3.

[9] W. Wang, A.F. Yu, J.Y. Zhai, Z.L. Wang, Recent Progress of Functional Fiber and Textile Triboelectric Nanogenerators: Towards Electricity Power Generation and Intelligent Sensing, Advanced Fiber Materials 3(6) (2021) 394-412. https://doi.org/10.1007/s42765-021-00077-9.

[10] S. Chen, Z.K. Wu, C.Z. Chu, Y.F. Ni, R.E. Neisiany, Z.W. You, Biodegradable Elastomers and Gels for Elastic Electronics, Advanced Science 9(13) (2022) 202105146.

https://doi.org/10.1002/advs.202105146.
[11] Z. Liu, H. Li, B.J. Shi, Y.B. Fan, Z.L. Wang, Z. Li, Wearable and Implantable Triboelectric Nanogenerators, Advanced Functional Materials 29(20) (2019) 201808820. https://doi.org/10.1002/adfm.201808820.
[12] M. Kim, H. Park, M.H. Lee, J.W. Bae, K.Y. Lee, J.H. Lee, J.H. Lee, Stretching-insensitive stretchable and biocompatible triboelectric nanogenerators using plasticized PVC gel and graphene electrode for body-integrated touch sensor, Nano Energy 107 (2023) 108159. https://doi.org/10.1016/j.nanoen.2022.108159.
[13] J.X. Jiang, Q.B. Guan, Y.N. Liu, X.H. Sun, Z. Wen, Abrasion and Fracture Self-Healable Triboelectric Nanogenerator with Ultrahigh Stretchability and Long-Term Durability, Advanced Functional Materials 31(47) (2021) 202105380. https://doi.org/10.1002/adfm.202105380.
[14] Y. Nurhamiyah, A. Amir, M. Finnegan, E. Themistou, M. Edirisinghe, B.Q. Chen, Wholly Biobased, Highly Stretchable, Hydrophobic, and Self-healing Thermoplastic Elastomer, ACS Applied Materials & Interfaces 13(5) (2021) 6720-6730. https://doi.org/10.1021/acsami.0c23155.
[15] H. Varghese, H.M.A. Hakkeem, K. Chauhan, E. Thouti, S. Pillai, A. Chandran, A high-performance flexible triboelectric nanogenerator based on cellulose acetate nanofibers and micropatterned PDMS films as mechanical energy harvester and self-powered vibrational sensor, Nano Energy 98 (2022) 107339. https://doi.org/10.1016/j.nanoen.2022.107339.
[16] K. Ghosh, C. Iffelsberger, M. Konecny, J. Vyskocil, J. Michalicka, M. Pumera, Nanoarchitectonics of Triboelectric Nanogenerator for Conversion of Abundant Mechanical Energy to Green Hydrogen, Advanced Energy Materials 13(11) (2023) 202203476. https://doi.org/10.1002/aenm.202203476.
[17] X. Feng, Q. Li, K. Wang, Waste Plastic Triboelectric Nanogenerators Using Recycled Plastic Bags for Power Generation, ACS Applied Materials & Interfaces 13(1) (2021) 400-410. https://doi.org/10.1021/acsami.0c16489.
[18] O.Y. Yue, X.C. Wang, M.D. Hou, M.H. Zheng, D.Y. Hao, Z.X. Bai, X.L. Zou, B.Q. Cui, C.L. Liu, X.H. Liu, Smart nanoengineered electronic-scaffolds based on triboelectric nanogenerators as tissue batteries for integrated cartilage therapy, Nano Energy 107 (2023) 108158. https://doi.org/10.1016/j.nanoen.2022.108158.
[19] S. Bi, X. Han, Q.Q. Chen, B.H. Gao, L.H. Chen, Z.R. He, C.M. Jiang, Ultralarge Curvature and Extreme Rapid Degradable Porous Wood Based Flexible Triboelectric Sensor for Physical Motion Monitoring, Advanced Materials Technologies 8(5) (2023) 202201066. https://doi.org/10.1002/admt.202201066.
[20] P. Ma, H.R. Zhu, H. Lu, Y.M. Zeng, N. Zheng, Z. Lin, X. Cao, Design of biodegradable wheat-straw based triboelectric nanogenerator as self-powered sensor for wind detection, Nano Energy 86 (2021) 106032. https://doi.org/10.1016/j.nanoen.2021.106032.
[21] Z.X. Wang, C. Chen, L. Fang, B. Cao, X.B. Tu, R.Y. Zhang, K. Dong, Y.C. Lai, P.H. Wang, Biodegradable, conductive, moisture-proof, and dielectric enhanced cellulose-based triboelectric nanogenerator for self-powered human-machine interface sensing, Nano Energy 107 (2023) 108151. https://doi.org/10.1016/j.nanoen.2022.108151.
[22] J.T. Zhang, S.M. Hu, Z.J. Shi, Y.F. Wang, Y.Q. Lei, J. Han, Y. Xiong, J. Sun, L. Zheng, Q.J. Sun, G. Yang, Z.L. Wang, Eco-friendly and recyclable all cellulose triboelectric nanogenerator and self-powered interactive interface, Nano Energy 89 (2021) 106354. https://doi.org/10.1016/j.nanoen.2021.106354.
[23] B. Luo, Q.Q. Zhou, W.Y. Chen, L.J. Sun, L. Yang, Y.F. Guo, H.J. Liu, Z.K. Wu, R.E. Neisiany, X.H. Qin, J. Pan, Z.W. You, Nonadjacent Wireless Electrotherapy for Tissue Repair by a 3D-Printed

Bioresorbable Fully Soft Triboelectric Nanogenerator, Nano Letters 23(7) (2023) 2927-2937. https://doi.org/10.1021/acs.nanolett.3c00300.

[24] S. Chen, T. Huang, H. Zuo, S.H. Qian, Y.F. Guo, L.J. Sun, D. Lei, Q.L. Wu, B. Zhu, C.L. He, X.M. Mo, E. Jeffries, H. Yu, Z.W. You, A Single Integrated 3D-Printing Process Customizes Elastic and Sustainable Triboelectric Nanogenerators for Wearable Electronics, Advanced Functional Materials 28(46) (2018) 201805108. https://doi.org/10.1002/adfm.201805108.

[25] J. Pansumdaeng, S. Kuntharin, V. Harnchana, N. Supanchaiyamat, Fully bio-based epoxidized soybean oil thermosets for high performance triboelectric nanogenerators, Green Chemistry 22(20) (2020) 6912-6921. https://doi.org/10.1039/d0gc01738h.

[26] D. Yang, Y.F. Ni, X.X. Kong, S.Y. Li, X.Y. Chen, L.Q. Zhang, Z.L. Wang, Self-Healing and Elastic Triboelectric Nanogenerators for Muscle Motion Monitoring and Photothermal Treatment, ACS Nano 15(9) (2021) 14653-14661. https://doi.org/10.1021/acsnano.1c04384.

[27] M. Tavakolizadeh, A. Pourjavadi, M. Ansari, H. Tebyanian, S.J.S. Tabaei, M. Atarod, N. Rabiee, M. Bagherzadeh, R.S. Varma, An environmentally friendly wound dressing based on a self-healing, extensible and compressible antibacterial hydrogel, Green Chemistry 23(3) (2021) 1312-1329. https://doi.org/10.1039/d0gc02719g.

[28] L.J. Sun, H.F. Huang, L.Z. Zhang, R.E. Neisiany, X.P. Ma, H. Tan, Z.W. You, Spider-Silk-Inspired Tough, Self-Healing, and Melt-Spinnable Ionogels, Advanced Science (2023) 202305697. https://doi.org/10.1002/advs.202305697.

[29] S.K. Ghosh, M.P. Kim, S. Na, Y. Lee, J. Park, S. Cho, J. Cho, J.J. Kim, H. Ko, Ultra-stretchable yet tough, healable, and biodegradable triboelectric devices with microstructured and ionically crosslinked biogel, Nano Energy 100 (2022) 107438. https://doi.org/10.1016/j.nanoen.2022.107438.

[30] H.L. Sheng, A.T. Zhu, L.H. Zhang, J. Huang, T.J. Yang, S.D. Qin, F.Z. Zhang, Q.Q. Xu, H.B. Xie, Use of an EMIM OAc /GVL-based organic electrolyte solvent to engineer chitosan into a nanocomposite organic ionogel electrolyte for flexible supercapacitors, Green Chemistry 25(8) (2023) 3046-3056. https://doi.org/10.1039/d2gc04019k.

[31] J.K. Wang, Y.Q. Deng, Z.Z. Ma, Y. Wang, S.Z. Zhang, L.F. Yan, Lignin promoted the fast formation of a robust and highly conductive deep eutectic solvent ionic gel at room temperature for a flexible quasi-solid-state supercapacitor and strain sensors, Green Chemistry 23(14) (2021) 5120-5128. https://doi.org/10.1039/d1gc01512e.

[32] Y.M. Liu, T.H. Wong, X.C. Huang, C.K. Yiu, Y.Y. Gao, L. Zhao, J.K. Zhou, W. Park, Z. Zhao, K.M. Yao, H. Li, H.L. Jia, J. Li, J.Y. Li, Y. Huang, M.G. Wu, B.B. Zhang, D.F. Li, C. Zhang, Z.K. Wang, X.E. Yu, Skin-integrated, stretchable, transparent triboelectric nanogenerators based on ion-conducting hydrogel for energy harvesting and tactile sensing, Nano Energy 99 (2022) 107442. https://doi.org/10.1016/j.nanoen.2022.107442.

[33] L.J. Sun, S. Chen, Y.F. Guo, J.C. Song, L.Z. Zhang, L.J. Xiao, Q.B. Guan, Z.W. You, Ionogel-based, highly stretchable, transparent, durable triboelectric nanogenerators for energy harvesting and motion sensing over a wide temperature range, Nano Energy 63 (2019) 103847. https://doi.org/10.1016/j.nanoen.2019.06.043.

[34] C.Y. Li, H.Y. Guo, Z.Y. Wu, P. Wang, D. Zhang, Y.H. Sun, Self-Healable Triboelectric Nanogenerators: Marriage between Self-Healing Polymer Chemistry and Triboelectric Devices, Advanced Functional Materials 33(2) (2023) 202208372. https://doi.org/10.1002/adfm.202208372.

[35] Y.J. Jia, L.Z. Zhang, M.L. Qin, Y. Li, S.J. Gu, Q.B. Guan, Z.W. You, Highly efficient self-healable and robust fluorinated polyurethane elastomer for wearable electronics, Chemical Engineering Journal

430 (2022) 133081. https://doi.org/10.1016/j.cej.2021.133081.
[36] C.Y. Jiang, L.Z. Zhang, Q. Yang, S.X. Huang, H.P. Shi, Q. Long, B. Qian, Z.H. Liu, Q.B. Guan, M.J. Liu, R.H. Yang, Q. Zhao, Z.W. You, X.F. Ye, Self-healing polyurethane-elastomer with mechanical tunability for multiple biomedical applications in vivo, Nature Communications 12(1) (2021) 4395. https://doi.org/10.1038/s41467-021-24680-x.
[37] B.-X. Cheng, J.-L. Zhang, Y. Jiang, S. Wang, H. Zhao, High Toughness, Multi-dynamic Self-Healing Polyurethane for Outstanding Energy Harvesting and Sensing, ACS applied materials & interfaces 15(50) (2023) 58806-58814. https://doi.org/10.1021/acsami.3c12384.
[38] H.L. Wang, Z.H. Guo, G. Zhu, X. Pu, Z.L. Wang, Boosting the Power and Lowering the Impedance of Triboelectric Nanogenerators through Manipulating the Permittivity for Wearable Energy Harvesting, ACS Nano 15(4) (2021) 7513-7521. https://doi.org/10.1021/acsnano.1c00914.
[39] O. Demircioglu, M.O. Cicek, D. Doganay, G. Gazaloglu, C. Baykal, S. Cinar, H.E. Unalan, Triboelectric nanogenerators for blue energy harvesting in simulated wave conditions, Nano Energy 107 (2023) 108157. https://doi.org/10.1016/j.nanoen.2022.108157.
[40] Z.H. Liu, L.Z. Zhang, Q.B. Guan, Y.F. Guo, J.M. Lou, D. Lei, S.L. Wang, S. Chen, L.J. Sun, H.X. Xuan, E.M. Jeffries, C.L. He, F.L. Qing, Z.W. You, Biomimetic Materials with Multiple Protective Functionalities, Advanced Functional Materials 29(28) (2019) 201901058. https://doi.org/10.1002/adfm.201901058.
[41] L.Z. Zhang, Q.B. Guan, A.O. Shen, R.E. Neisiany, Z.W. You, M.F. Zhu, Supertough spontaneously self-healing polymer based on septuple dynamic bonds integrated in one chemical group, Science China-Chemistry 65(2) (2022) 363-372. https://doi.org/10.1007/s11426-021-1157-9.
[42] L.Z. Zhang, Z.H. Liu, X.L. Wu, Q.B. Guan, S. Chen, L.J. Sun, Y.F. Guo, S.L. Wang, J.C. Song, E.M. Jeffries, C.L. He, F.L. Qing, X.G. Bao, Z.W. You, A Highly Efficient Self-Healing Elastomer with Unprecedented Mechanical Properties, Advanced Materials 31(23) (2019) 201901402. https://doi.org/10.1002/adma.201901402.
[43] Y. Yang, D. Lei, S.X. Huang, Q. Yang, B.Y. Song, Y.F. Guo, A. Shen, Z.Z. Yuan, S. Li, F.L. Qing, X.F. Ye, Z.W. You, Q. Zhao, Elastic 3D-Printed Hybrid Polymeric Scaffold Improves Cardiac Remodeling after Myocardial Infarction, Advanced Healthcare Materials 8(10) (2019) 201900065. https://doi.org/10.1002/adhm.201900065.
[44] S. Chen, L.J. Sun, X.J. Zhou, Y.F. Guo, J.C. Song, S.H. Qian, Z.H. Liu, Q.B. Guan, E.M. Jeffries, W.G. Liu, Y.D. Wang, C.L. He, Z.W. You, Mechanically and biologically skin-like elastomers for bio-integrated electronics, Nature Communications 11(1) (2020) 1107. https://doi.org/10.1038/s41467-020-14446-2.
[45] H. Tan, L. Sun, H. Huang, L. Zhang, R.E. Neisiany, X. Ma, Z. You, Continuous Melt Spinning of Adaptable Covalently Cross-Linked Self-Healing Ionogel Fibers for Multi-Functional Ionotronics, Advanced materials (2023) e2310020. https://doi.org/10.1002/adma.202310020.
[46] H. Tan, L.Z. Zhang, X.P. Ma, L.J. Sun, D.L. Yu, Z.W. You, Adaptable covalently cross-linked fibers, Nature Communications 14(1) (2023) 2218. https://doi.org/10.1038/s41467-023-37850-w.
[47] L. Sun, H. Huang, Q. Guan, L. Yang, L. Zhang, B. Hu, E. Neisiany Rasoul, Z. You, M. Zhu, Cooperative Chemical Coupling and Physical Lubrication Effects Construct Highly Dynamic Ionic Covalent Adaptable Network for High- Performance Wearable Electronics, CCS Chemistry 5(5) (2023) 1096-1107. https://doi.org/10.31635/ccschem.022.202202037.
[48] P.L. Jiaxin Dou, Yuancong Zhao, Lei Zhou, Xin Li, Jin Wang, Nan Huang, Copper-mediated polyurethane materials with enzyme-like catalysis for biocompatibility improvement in blood

environments, Biosurface and Biotribology (2021) 1-12. https://doi.org/10.1049/bsb2.12009.
[49] H. Tan, M. Guo, R.N. Du, X.Y. Xie, J.H. Li, Y.P. Zhong, Q. Fu, The effect of fluorinated side chain attached on hard segment on the phase separation and surface topography of polyurethanes, Polymer 45(5) (2004) 1647-1657. https://doi.org/10.1016/j.polymer.2003.12.064.
[50] G.E. Fantner, T. Hassenkam, J.H. Kindt, J.C. Weaver, H. Birkedal, L. Pechenik, J.A. Cutroni, G.A.G. Cidade, G.D. Stucky, D.E. Morse, P.K. Hansma, Sacrificial bonds and hidden length dissipate energy as mineralized fibrils separate during bone fracture, Nature Materials 4(8) (2005) 612-616. https://doi.org/10.1038/nmat1428.
[51] H.L. Xu, S.W. Zhao, A.Q. Yuan, Y.L. Zhao, X.D. Wu, Z.K. Wei, J.X. Lei, L. Jiang, Exploring Self-Healing and Switchable Adhesives based on Multi-Level Dynamic Stable Structure, Small (2023) 202300626. https://doi.org/10.1002/smll.202300626.
[52] Y.J. Li, D. Yang, Z.Y. Wu, F.L. Gao, X.Z. Gao, H.Y. Zhao, X.F. Li, Z.Z. Yu, Self-adhesive, self-healing, biocompatible and conductive polyacrylamide nanocomposite hydrogels for reliable strain and pressure sensors, Nano Energy 109 (2023) 108324. https://doi.org/10.1016/j.nanoen.2023.108324.
[53] Y.J. Li, Z.Y. Tian, X.Z. Gao, H.Y. Zhao, X.F. Li, Z.L. Wang, Z.Z. Yu, D. Yang, All-Weather Self-Powered Intelligent Traffic Monitoring System Based on a Conjunction of Self-Healable Piezoresistive Sensors and Triboelectric Nanogenerators, Advanced Functional Materials 33(52) (2023) 202308845. https://doi.org/10.1002/adfm.202308845.
[54] J.W. Chen, H.J. Wang, Y.J. Wu, Y.J. Liu, Y.W. Shi, C.S. Chen, H.G. Hou, Z.G. Zha, X.F. Zheng, T.T. Wu, Biocompatible octacalcium phosphate/sodium alginate/silk fibroin composite scaffolds for bone regeneration, Materials Today Communications 31 (2022) 103312. https://doi.org/10.1016/j.mtcomm.2022.103312.
[55] B. Zhang, L. Ma, L.S. Tang, D.W. Song, J. Guo, F. Zhang, X. Xu, In vitro and in vivo evaluation of a modified porcine acellular dermal matrix for soft tissue augmentation, Journal of Biomaterials Applications 37(8) (2023) 1497-1506. https://doi.org/10.1177/08853282221140667.
[56] X. Xiao, X.C. Meng, D. Kim, S. Jeon, B.J. Park, D.S. Cho, D.M. Lee, S.W. Kim, Ultrasound-Driven Injectable and Fully Biodegradable Triboelectric Nanogenerators, Small Methods 7(6) (2023) 202201350. https://doi.org/10.1002/smtd.202201350.
[57] W.Y. Zhang, Q. Liu, S.Y. Chao, R.P. Liu, X. Cui, Y. Sun, H. Ouyang, Z. Li, Ultrathin Stretchable Triboelectric Nanogenerators Improved by Postcharging Electrode Material, ACS Applied Materials & Interfaces 13(36) (2021) 42966-42976. https://doi.org/10.1021/acsami.1c13840.
[58] Z. Wen, Y.Q. Yang, N. Sun, G.F. Li, Y.N. Liu, C. Chen, J.H. Shi, L.J. Xie, H.X. Jiang, D.Q. Bao, Q.Q. Zhuo, X.H. Sun, A Wrinkled PEDOT:PSS Film Based Stretchable and Transparent Triboelectric Nanogenerator for Wearable Energy Harvesters and Active Motion Sensors, Advanced Functional Materials 28(37) (2018) 201803684. https://doi.org/10.1002/adfm.201803684.
[59] S. Sriphan, N. Vittayakorn, Facile roughness fabrications and their roughness effects on electrical outputs of the triboelectric nanogenerator, Smart Materials and Structures 27(10) (2018) 105026. https://doi.org/10.1088/1361-665X/aadb65.
[60] J. Wen, H.L. He, C.P. Niu, M.Z. Rong, Y.Q. Huang, Y. Wu, An improved equivalent capacitance model of the triboelectric nanogenerator incorporating its surface roughness, Nano Energy 96 (2022) 107070. https://doi.org/10.1016/j.nanoen.2022.107070.
[61] L.L. Liu, D. Zhang, P.J. Bai, Y. Mao, Q. Li, J.Q. Guo, Y.J. Fang, R.J. Ma, Strong Tough Thermogalvanic Hydrogel Thermocell With Extraordinarily High Thermoelectric Performance, Advanced Materials 35(32) (2023) 202300696. https://doi.org/10.1002/adma.202300696.

[62] D. Zhang, Q. Li, Y.J. Fang, P.J. Bai, L.L. Liu, J.Q. Guo, G.F. Wang, Y.T. Zhou, R.J. Ma, High-performance wood-based thermoelectric sponges for thermal energy harvesting and smart buildings, Nano Research (2024) 12274. https://doi.org/10.1007/s12274-024-6467-y.